Generation of Ramped Current Profiles in Relativistic Electron Beams Using Wakefields in Dielectric Structures

G. Andonian,[1,2] S. Barber,[1] F. H. O'Shea,[2] M. Fedurin,[3] K. Kusche,[3] C. Swinson,[3] and J. B. Rosenzweig[1]
[1]Department of Physics and Astronomy, UCLA, Los Angeles, California 90095, USA
[2]RadiaBeam Technologies, Santa Monica, California 90404, USA
[3]Accelerator Test Facility, Brookhaven National Laboratory, Upton, New York 11973, USA
(Received 8 April 2016; published 3 February 2017)

Temporal pulse tailoring of charged-particle beams is essential to optimize efficiency in collinear wakefield acceleration schemes. In this Letter, we demonstrate a novel phase space manipulation method that employs a beam wakefield interaction in a dielectric structure, followed by bunch compression in a permanent magnet chicane, to longitudinally tailor the pulse shape of an electron beam. This compact, passive, approach was used to generate a nearly linearly ramped current profile in a relativistic electron beam experiment carried out at the Brookhaven National Laboratory Accelerator Test Facility. Here, we report on these experimental results including beam and wakefield diagnostics and pulse profile reconstruction techniques.

DOI: 10.1103/PhysRevLett.118.054802

The development of next-generation light sources and colliders hinges on advances in high-energy, high-gradient field generation beyond conventional radio-frequency (rf) acceleration. Alternative acceleration techniques are required for deployment of high-brightness beams in a manageable footprint, and cost-effective manner. Charged particle beam-driven wakefield schemes, such as dielectric wakefield acceleration (DWA) or plasma wakefield acceleration, are anticipated candidates to progress the field with the promise of multi-GV/m accelerating gradients [1–3]. However, the viability of collinear, beam-driven wakefield schemes for such applications depends on demonstrated enhanced extracted energy efficiency, typically characterized by the transformer ratio $\mathcal{R}$. The transformer ratio, for the collinear beam-driven wakefield accelerator, is defined as the ratio between the peak acceleration field behind the driving bunch and the peak decelerating field experienced by the bunch. For symmetric bunch profiles, $\mathcal{R} < 2$; however, specially shaped asymmetric profiles, such as a longitudinally linearly ramped (i.e., triangular) shape, allow for greater $\mathcal{R}$ [4–6].

Existing robust methods to shape the longitudinal profile of the beam include higher-order magnetic compensation [7,8] and notch collimation [9] in high-dispersion beam lines, direct drive laser pulse shaping [10], or transverse to longitudinal emittance exchange techniques [11,12]. In this Letter we describe and demonstrate an alternative bunch shaping scheme that uses a beam wakefield interaction in a dielectric lined structure, followed by a compact chicane, to generate approximately linearly ramped distributions. The method is advantageous to other beam shaping techniques as it has a compact footprint, is passive (i.e., requires no external power source), can be placed close to the interaction region to alleviate profile preservation issues in transport [13], and does not reduce charge through masking techniques allowing for the utilization of the full beam charge. The approach is also scalable to higher energies.

In this concept, a charged particle bunch traverses through a dielectric lined structure producing a wakefield. For Gaussian beams with a rms bunch length on the order of $\sim 1/4$ of the excited wakefield wavelength, an energy correlation is imparted onto the trailing distribution of the beam that samples only the leading, decelerating component of the wakefield. The energy-time correlation is then converted to a density modulation via a magnetic chicane compressor, whose strength is characterized by the longitudinal dispersion, given by the matrix element of the transport function corresponding to the beam energy-path length correlation, R_{56}. The resultant current profile of the bunch is a nearly linearly ramped, or triangular, distribution, with many parameters available for optimization (dielectric material, shape, size, chicane R_{56}) as depicted schematically in Fig. 1 [14]. This method follows similar lines of recent work on dielectric structures used for beam and radiation manipulations, such as sources for narrow band terahertz radiation, beam dechirpers, and microbunchers [15–17]. For example, in the opposite limit, where the driver beam bunch length is much longer than the wakefield wavelength, the dielectric wakefield interaction can be used to produce microbunched beamlet distributions [18].

For a charged bunch traveling through a dielectric lined waveguide, the wakefield is a convolution of its wake function with the longitudinal profile distribution [4]

$$W(z) = -\int_0^\infty \rho(z - z')w(z')dz, \tag{1}$$

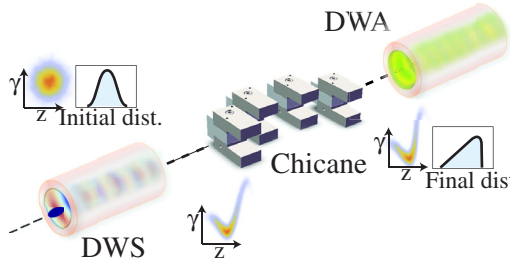

FIG. 1. Conceptual schematic for ramped bunch generation, with insets of longitudinal phase space and current profiles (not to scale). A dielectric wakefield "shaper" (DWS) imposes a partial sinusoidal energy correlation on the drive beam dependent on the frequency supported by the structure. The chicane converts this correlation into density space. The resultant profile is linearly ramped ready for injection into an, e.g., dielectric wakefield accelerator (of different frequency) for enhanced efficiency with high $\mathcal{R}$.

where $\rho(z)$ is the normalized longitudinal bunch distribution, and $w(z)$ is the wake function, which for a single-mode, cylindrically symmetric, dielectric lined structure is given by

$$w(z) = \frac{Z_0 c}{\pi a^2} \cos kz \tag{2}$$

with Z_0 the impedance of free space, c the speed of light in vacuum, a the inner radius of the dielectric structure, and k the wave number corresponding to the fundamental mode of the structure (e.g., TM_{01} for a cylindrical structure), which is calculated by solving the dispersion relation for a dielectric lined cylindrical waveguide. The energy change $\delta E = E - E_0$ of a given particle of energy E from initial energy E_0 is proportional to the wakefield induced voltage for a given net charge of Nq_e, over an interaction distance of L_d, where N and q_e are the total number of electrons and electron charge, respectively. For small fractional energy deviation, δ_E is given by [4]

$$\delta E(z) = q_e(Nq_e)W(z)L_d. \tag{3}$$

After passing through the dielectric structure, the linear coordinate transformation in phase space for a chicane of given R_{56} is simply $z = z_0 + R_{56}(\delta E/E_0)$. In practice, the dielectric structure is designed such that the fundamental wavelength supported by the structure is approximately 4 times the bunch length of the drive beam. Conceptually, this scaling is necessary so that the bulk of the beam experiences only the leading decelerating component of the wakefield that is generated as it passes through the structure. For appropriate values of fundamental frequency, the chicane, characterized by its R_{56} value, alters the longitudinal phase space to generate a nearly linearly ramped current profile after passage through the transport.

TABLE I. Measured experimental parameters for the electron beam and dielectric structure.

Beam energy (E_0)	50 MeV
Energy spread (δ_E/E_0)	1×10^{-4}
Total charge (Nq_e)	80 pC
Normalized emittance (ϵ_n)	2 mm mrad
Transverse spot size (σ_r)	60 μm
rms bunch length (σ_z)	180 μm
Dielectric structure inner (outer) radius a (b)	200 (300) μm
Dielectric structure length (L_d)	5 cm
Dielectric constant (ϵ)	3.8
Fundamental mode (f_{01})	0.39 THz
Chicane strength (R_{56})	9.2 mm

An experiment to generate ramped bunch distributions using the described method was carried out at the Brookhaven National Laboratory (BNL) Accelerator Test Facility (ATF). The BNL ATF electron beam parameters used for this experiment are listed in Table I. The initial distribution is approximately Gaussian in the longitudinal coordinate with a correlated energy chirp [Fig. 2 (left)]. The analytically calculated beam phase space distribution after interaction with the generated wakefield, using the transformation described by Eq. (3), is shown in Fig. 2 (middle). The longitudinal phase space correlation shows that the particle distribution is partially sinusoidal in energy due to the wakefield interaction; however, the current profile is still Gaussian. The chicane compressor transformation serves to shear the phase space, manifesting in a particle density correlation. The final distribution and current profiles are shown in Fig. 2 (right) where the current profile is approximately triangular.

Accurately satisfying the shaping criterion requires exact calculation of the fundamental frequency dependent on the dielectric structure parameters. The fundamental operating frequency of a cylindrically symmetric, dielectric lined structure can be determined from the solution to the transcendental equation describing the generated wakefield, as in Ref. [19], where $a(b)$ is the inner (outer) radius of the dielectric cylinder, $(b - a)$ is the thickness of the dielectric, and ϵ is the relative permittivity. The design rms bunch length of the BNL ATF experiment is $\sigma_z = 180$ μm and the dielectric structure with frequency $f_{01} = 0.39$ THz ($\lambda_{01} = 765$ μm) was used.

The cylindrical dielectric structure is composed of SiO_2 ($\epsilon = 3.8$), with $a(b) = 200(300)$ μm and a 25 μm thick copper coating, deposited with a multistep process consisting of a thin titanium adhesion layer, followed by a thin copper transition layer, and a bulk electroplated deposition of copper. The structure is mounted on an *in situ* aluminum holder and a multiaxis, remote control stage for final precision alignment. The chicane in this experiment is composed of four permanent magnet (NdFeB) dipoles, 10 cm long, with a 7.5 mm gap, and a typical field on the

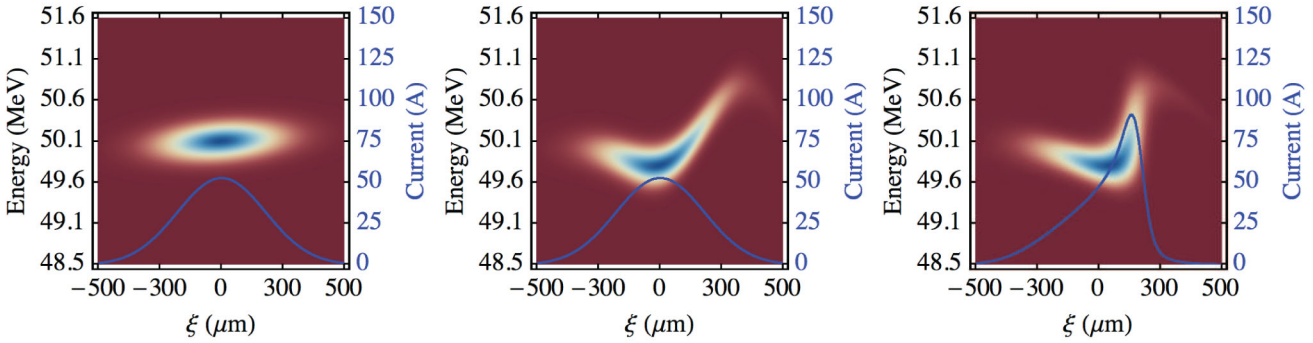

FIG. 2. Longitudinal phase space describing correlation with the particle energy and longitudinal coordinate ($\xi = z - z_0$), in false color for the initial Gaussian beam distribution (left), after interaction with the wakefield in the dielectric structure (middle), and after compression in the chicane (right). The current profile for each distribution is superimposed on the intensity plot, with conversion to the desired approximately triangular distribution at the end of the transformation. The parameters used here correspond to the beam measurements from BNL ATF.

order of 8 kG assembled on an aluminum strongback. Aluminum spacers provide precision offset and the design R_{56} is tuned on a bench top while zeroing the effects of the first and second integrals of the magnetic field and using nonmagnetic shims. The measured R_{56} for this chicane is 9.2 mm.

For these measurements, the BNL ATF produced an electron beam with bunch length σ_z variable in the range of 150–200 μm, which was propagated to an interaction point in a dedicated experimental chamber that housed the dielectric structure and chicane compressor. The design rms bunch length was $\sigma_z = 180$ μm. The dielectric structure and chicane are aligned to the electron beam centroid trajectory as mapped on insertable transverse profile monitors, using a local visible alignment laser, focussed down to a ~40 μm spot size at the interaction point. The beam line and diagnostic components have been described in detail in Refs. [18,20,21]. The beam line utilizes a doublet and triplet quadrupole configuration for electron beam final focus and collimation into the experimental chamber. The beam energy spectrum is diagnosed using a dipole and screen with a high-resolution CCD located at the beam dump. The beam charge is monitored using a Faraday cup, and the emittance is measured using a parameter fitting routine to transverse beam sizes along the transport measured with scintillating beam profile monitors. The beam spot size is measured using a four-screen method with profile monitors positioned around the interaction region. The relevant measured beam parameters for this experiment are summarized in Table I.

The electron beam current profile distributions are measured using coherent transition radiation (CTR) interferometric methods for cases of the beam traversal with and without the wakefield shaping device. CTR carries frequency information directly related to the longitudinal beam form factor and such methods are commonly used in accelerator facilities to determine beam bunch profiles [22]. In this study, the measurements are performed using CTR generated from the electron beam incident upon a 45 deg polished aluminum mirror located ~10 cm downstream of the chicane exit. The CTR is reflected to a Michelson-like terahertz-band interferometer and He-cooled silicon bolometer detector, where the signal is autocorrelated. A typical autocorrelation scan consists of stepping the optical path length delay in 40 μm increments over a total length of 4 mm and averaging four shots per step.

Using the analytical profile distributions of Fig. 2, the predicted CTR autocorrelations of an unperturbed beam, and a beam interacting with the wakefield shaping components, are shown in Fig. 3. These results include effects of frequency cutoffs from the transport and detector. Some noticeable signatures are evident. First, in the case of the ramped beam, the central peak is slightly narrower with a higher peak value indicating a compression process. Second, the ramped beam shows additional higher frequency components, with longer roll-off, as indicated in the spectra when taking the FFT of the autocorrelation curves [Fig. 3 (right)].

The experimentally measured autocorrelations [Fig. 4 (left)] and FFTs [Fig. 4 (center)], both with and without passage through the dielectric wakefield shaping setup, reveal signatures that are predicted from the calculations shown in Fig. 3, namely, a narrower central peak with a

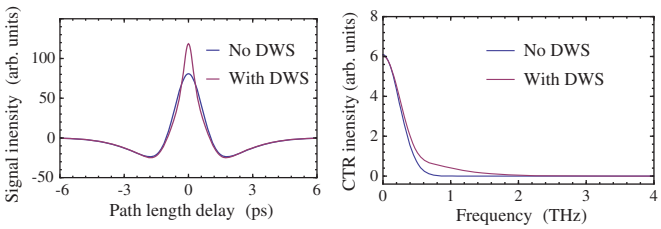

FIG. 3. Left: predicted autocorrelation traces using the simulated current profiles of Fig. 2 for the unperturbed beam (blue) and the beam going through the dielectric wakefield shaper (red). Right: FFT of the corresponding autocorrelation curves.

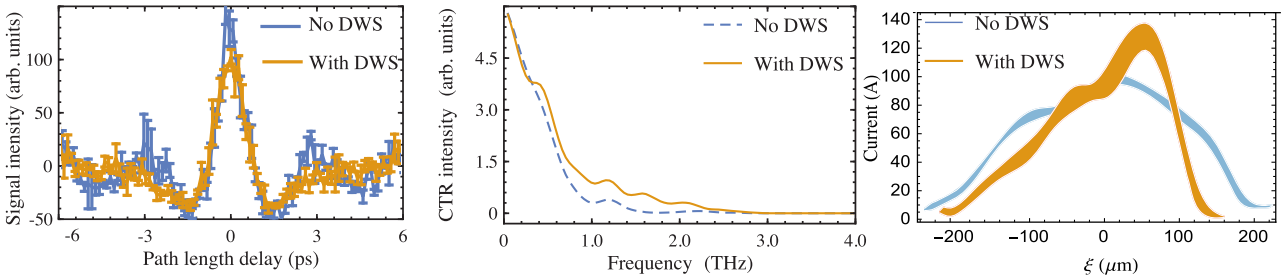

FIG. 4. Left: autocorrelation measurements at the BNL ATF for the cases where the beam is unperturbed (blue curve) and when the beam traverses through the dielectric wakefield shaping (DWS) structures (yellow curve). Each step along the autocorrelation consists of four shots (range shown by error bars). Middle: frequency spectra for the two cases using the average values of the autocorrelation plots. Right: full pulse reconstructions of the unperturbed beam and the shaped beam, with width of shading on curve showing the variance of >1000 different reconstructions with random cutoff frequency within confidence intervals.

greater amplitude, and longer high-frequency roll-off at ~1 THz, that is consistent for the linearly ramped case compared to the symmetric case. These features of the raw autocorrelations themselves represent necessary qualitative agreement of the linear current profiles; however, the full current profile distributions, with more detailed information, are performed using a CTR interferometry reconstruction algorithm.

In principle, the longitudinal profile of a single electron beam can be reconstructed from the CTR emission intensity spectrum using the Kramers-Kronig relations and a minimal phase assumption, if the entire frequency spectrum is known [23]. In practice, however, experimental factors limit the ability to wholly measure the spectrum across the full range from zero to infinity. Hence, informed by other experimental measurements, the missing frequency components of the spectrum must be augmented for accurate bunch length reconstruction. The low-frequency cutoff is related to several factors such as detector sensitivity and diffraction through the quasioptical collection transport. This systematic response, however, can be approximately calibrated in whole by analyzing the CTR emission response. The time domain autocorrelation of the CTR generated by a short bunch, as in the measurement described herein, exhibits characteristic dips on either side of the central peak, which are due to the systematic low frequency cutoff. This cutoff is modeled with an analytic filter function, as motivated in Ref. [22], with the form $g(\omega) = 1 - e^{-\zeta^2\omega^2}$, where ζ^{-1} is the characteristic cutoff frequency calculated from a fit to the measured CTR autocorrelation curve of the given bunch length. The subsequent spectral measurements are divided by this filter function, to effectively restore the low frequency spectral amplitude. For these experimental measurements, the cutoff frequency determined from the nonlinear regression (fit) to the CTR model is 108 GHz, with a standard deviation of 4 GHz and a 95% confidence interval of 100–115 GHz. Additionally, at high-frequency, the spectral amplitude of CTR generated by a short bunch rapidly drops to zero for wavelengths shorter than the bunch. In the measured spectra there is a white noise frequency response well above this coherent regime, which must be subtracted as background, to eliminate the influence of spurious artifacts in the reconstruction.

Once all frequencies are accounted for, the Kramers-Kronig transform is used to inform on the complex phase term of the frequency dependent form factor. The longitudinal bunch distribution is then evaluated from the Fourier transform of the complex form factor following the analysis in Ref. [23]. The measured data sets, with the restored frequencies as described above, are shown in Fig. 4 (center), and used to calculate the phase factor. The spectra in Fig. 3 (right) show the difference in the expected spectral characteristics for the asymmetric ramped beam relative to the input beam. The relative frequency falloff and higher frequency content expected near ~1 THz, manifests as an additional skewness to the final distribution, as seen in the data in Fig. 4 (right). The calculated frequency dependent phase term, which informs on the asymmetry of the bunch, and amplitude are then used to generate the longitudinal form factor used in the profile reconstruction. Figure 4 (right) shows the end result of the reconstruction algorithm for the two cases. The distribution for the shaped beam is shown to be ramped with a high level of skewness, relative to the initial bunch distribution, which is consistent with the analytical theory and predicted models from the simulation results shown above.

At this point in the analysis, it is important to evaluate how possible errors in the assumptions used to augment the full frequency domain may propagate through the reconstruction algorithm and lead to different bunch profiles in the time domain for the given data sets. Figure 4 (left) shows the measured autocorrelation curves including error bars that denote the measurement ranges of maximum and minimum values for each time step during the autocorrelation scan. The average values for each curve are Fourier transformed to generate the spectra. The shading on the curves of Fig. 4 (right) shows the results of the reconstruction algorithm run for >1000 cases in which the low frequency restoration is slowly changed by

varying the characteristic ζ over a range within the confidence interval, and the noise subtraction is varied over a range informed by the rms value of the measured noise amplitude. The results of this analysis demonstrate the algorithm robustness in terms of variations in the observed data and variations in the previously discussed assumptions required to perform the bunch shape reconstruction.

In summary, an experiment to tailor beam current profiles using a wakefield interaction in a dielectric structure was carried out at the BNL ATF. The results showed that nearly linearly ramped current profile generation of relativistic electron beams was measurable with existing diagnostics and robust reconstruction algorithms, in a compact, passive layout. Follow-on experiments to realize and measure the transformer ratio are presently underway and preliminary simulations show that using the shaped pulse from this experiment, followed by a dielectric wakefield accelerating structure of higher frequency, will yield an enhanced $\mathcal{R}$ compared to the unpurterbed beam. Further, measurements using a nascent transverse deflecting cavity for profile diagnosis [24] will allow for single-shot, real-time optimization of the ramped beam for injection into an accelerating module. Phase space manipulations using beam-driven dielectric wakefield structures, such as those presented here, show promise as real tools applicable in present-day and future accelerators. Such shaping schemes are adaptable and scalable for future high-energy colliders and next generation light sources based on advanced accelerator methods [25].

This work supported by DOE SBIR Grant No. DE-SC0011271 and DOE HEP Grant No. DE-SC0009914. The authors acknowledge useful discussions and contributions from P. Frigola, P. Hoang, A. Murokh, P. Musumeci, B. O'Shea, and O. Williams. This research used resources of the BNL ATF, which is a U.S. Department of Energy Office of Science User Facility.

[1] M. Thompson, H. Badakov, A. Cook, J. Rosenzweig, R. Tikhoplav, G. Travish, I. Blumenfeld, M. Hogan, R. Ischebeck, N. Kirby *et al.*, Phys. Rev. Lett. **100**, 214801 (2008).

[2] M. Litos, E. Adli, W. An, C. I. Clarke, C. E. Clayton, S. Corde, J. P. Delahaye, R. J. England, A. S. Fisher, J. Frederico *et al.*, Nature (London) **515**, 92 (2015).

[3] B. D. O'Shea, G. Andonian, S. K. Barber, K. L. Fitzmorris, S. Hakimi, J. Harrison, P. D. Hoang, M. J. Hogan, B. Naranjo, O. B. Williams *et al.*, Nat. Commun. **7**, 12763 (2016).

[4] K. L. F. Bane, P. Chen, and P. Wilson, SLAC Tech. Note, SLAC-PUB-3662 (1985).

[5] B. Jiang, J. Power, R. Lindberg, W. Liu, and W. Gai, Phys. Rev. Lett. **106**, 114801 (2011).

[6] F. Lemery and P. Piot, Phys. Rev. ST Accel. Beams **18**, 081301 (2015).

[7] R. J. England, J. B. Rosenzweig, G. Andonian, P. Musumeci, G. Travish, and R. Yoder, Phys. Rev. ST Accel. Beams **8**, 012801 (2005).

[8] R. J. England, J. B. Rosenzweig, and G. Travish, Phys. Rev. Lett. **100**, 214802 (2008).

[9] P. Muggli, V. Yakimenko, M. Babzien, E. K. Kallos, and K. P. Kusche, Phys. Rev. Lett. **101**, 054801 (2008).

[10] G. Penco, M. Danailov, A. Demidovich, E. Allaria, G. De Ninno, S. Di Mitri, W. M. Fawley, E. Ferrari, L. Giannessi, and M. Trovó, Phys. Rev. Lett. **112**, 044801 (2014).

[11] P. Piot, C. Behrens, C. Gerth, M. Dohlus, F. Lemery, D. Mihalcea, P. Stoltz, and M. Vogt, Phys. Rev. Lett. **108**, 034801 (2012).

[12] D. Xiang and A. Chao, Phys. Rev. ST Accel. Beams **14**, 114001 (2011).

[13] D. Y. Shchegolkov and E. I. Simakov, Phys. Rev. ST Accel. Beams **17**, 041301 (2014).

[14] G. Andonian, F. O'Shea, S. Barber, and J. Rosenzweig, AIP Conf. Proc. **1777**, 070002 (2016).

[15] G. Andonian, O. Williams, S. Barber, D. Bruhwiler, P. Favier, M. Fedurin, K. Fitzmorris, A. Fukasawa, P. Hoang, K. Kusche *et al.*, Phys. Rev. Lett. **113**, 264801 (2014).

[16] F. Lemery and P. Piot, Phys. Rev. ST Accel. Beams **17**, 112804 (2014).

[17] S. Antipov, S. Baturin, C. Jing, M. Fedurin, A. Kanareykin, C. Swinson, P. Schoessow, W. Gai, and A. Zholents, Phys. Rev. Lett. **112**, 114801 (2014).

[18] S. Antipov, C. Jing, M. Fedurin, W. Gai, A. Kanareykin, K. Kusche, P. Schoessow, V. Yakimenko, and A. Zholents, Phys. Rev. Lett. **108**, 144801 (2012).

[19] A. M. Cook, R. Tikhoplav, S. Y. Tochitsky, G. Travish, O. B. Williams, and J. B. Rosenzweig, Phys. Rev. Lett. **103**, 095003 (2009).

[20] G. Andonian, O. Williams, X. Wei, P. Niknejadi, E. Hemsing, J. B. Rosenzweig, P. Muggli, M. Babzien, M. Fedurin, K. Kusche *et al.*, Appl. Phys. Lett. **98**, 202901 (2011).

[21] G. Andonian, D. Stratakis, M. Babzien, S. Barber, M. Fedurin, E. Hemsing, K. Kusche, B. O'Shea, X. Wei, O. Williams *et al.*, Phys. Rev. Lett. **108**, 244801 (2012).

[22] A. Murokh, J. Rosenzweig, M. Hogan, H. Suk, G. Travish, and U. Happek, Nucl. Instrum. Methods Phys. Res., Sect. A **410**, 452 (1998).

[23] R. Lai and A. J. Sievers, Phys. Rev. E **50**, R3342 (1994).

[24] A. Murokh *et al.*, in *Proceedings of European Particle Accelerator Conference 2008 (EPAC'08), Genoa, Italy, 2008* (JACoW, Geneva, 2008), p. 1215.

[25] A. Zholents, W. Gai, R. Lindberg, J. G. Power, Y. Sun, C. Jing, A. Kanareykin, C. Li, C. X. Tang, D. Y. Shchegolkov *et al.*, in *Proceedings of Free Electron Conference 2014 (FEL2014), Basel, Switzerland, 2014* (JACoW, Geneva, 2014), p. 993.